Hindawi Publishing Corporation
Journal of Nanomaterials
Volume 2013, Article ID 826816, 5 pages
http://dx.doi.org/10.1155/2013/826816

Research Article

Pores and Microanalysis of Microbe-Inspired Nano-$CaCO_3$ Cementing Sand Columns

Li Li,[1] Qian Chunxiang,[2] and Zhao Yonghao[3]

[1] *School of Materials Science and Engineering, Nanjing University of Science and Technology, Street of Xiao Ling Wei 200, Nanjing, Jiangsu 210009, China*
[2] *East of Ji Yin Da Dao, School of Materials Science and Engineering, Southeast University, Jiangning Nanjing, Jiangsu 211189, China*
[3] *Nano-Structural Materials Center, School of Materials Science and Engineering, Nanjing University of Science and Technology, Street of Xiao Ling Wei 200, Nanjing, Jiangsu 210009, China*

Correspondence should be addressed to Li Li; lili_smse@njust.edu.cn

Received 5 September 2013; Revised 4 November 2013; Accepted 4 November 2013

Academic Editor: Hui Xia

This paper introduced an innovative bioengineering method of consolidating incompact sand by urea hydrolysis producing calcite cementation under the inducement of reproductive urease microbe. The result of mercury intrusion porosimetry showed the pore volume fractions of sand columns cemented by microbe-inspired nano-$CaCO_3$ on an accelerating reduction during the time of cementation, the process of which represented the bulk density of nano-$CaCO_3$ cementing sand columns that reinforced themselves positively all the time. The white precipitate particles exhibited a uniformed distribution of about 15 μm size and of a hexahedral shape mostly under SEM. Based on the Scherrer equation, the crystallite size of the white precipitate was calculated for 18.5 nm. The diffraction pattern of the white precipitate under TEM was taken in alignment with the 52 inorganic crystal composed of three elements of Ca, C, and O in PCPDFWIN-2000 and the precipitate was identified as ID86-2334 calcite calcium carbonate.

1. Introduction

Biomineralization is discovered and applied in geological material consolidation [1, 2]. With the application of this discovery to sand biocementation as the in situ microinspired calcite precipitation technique (MCP technique for abbreviation), a solution of urease-productive bacteria and urea was mixed and calcium chloride was first injected in sand and then in bacteria-producing urease dehydrates urea, shown in (1) and (2), and consequently calcium carbonate precipitates and fills in the spacing of sand, shown in (3) and (4):

$$CO(NH_2)_2 + H_2O \xrightarrow{\text{bacteria}} NH_2COOH + NH_3 \quad (1)$$

$$NH_2COOH + H_2O \longrightarrow NH_3 + H_2CO_3 \quad (2)$$

$$H_2CO_3 \longleftrightarrow 2H^+ + CO_3^{2-} \quad (3)$$

$$Ca^{2+} + CO_3^{2-} \longleftrightarrow CaCO_3 \downarrow \quad (4)$$

Microstructure analysis was made by the formulas of XRD, TEM, and SEM, combined with mercury intrusion porosimetry method to investigate the $CaCO_3$ particles size distributions and locations. This paper focused on the characterization of nano-$CaCO_3$ precipitate itself and its influence on sand-based material properties.

2. Materials and Methods

2.1. Microorganism and Growth Conditions. Liquid culture media consisting of 3 g/L nutrient broth, 5 g/L peptone, and 2.4 g/L urea were adjusted to pH 7.0 and sterilized for 25 min at 121°C. 2 mL (OD600 nm = 0.8). *Bacillus pasteurii* (isolated and preserved appropriately in our lab) were added into 100 mL culture medium and incubated at 30°C at 170 rpm for 24 hours in the shaker (XinZhi, China) [3].

2.2. Microbe-Inspired Nano-$CaCO_3$-Sand Cementation. 15 g of sand in 200 μm diameter was added with appropriate

Table 1: Calculated porosity structure factors of MIP data report of sand columns.

No.	Days/d	Grades	Permeable area/10^{-3} μm^2	Total porosity/%	Pore volume/mL/g	Specific area/m^2/m	Pore throat/pore
A1	5	Super low	0.08356	40.466	0.2500	0.0166	3.8286
A9	10	Super low	0.11084	35.724	0.2119	0.0169	4.1489
A13	15	Super low	0.03961	35.538	0.2137	0.0186	2.8909
A20	20	Super low	0.01479	27.855	0.1437	0.0236	3.8554
A27	28	Super low	0.00044	27.305	0.1394	0.1170	0.4865
B1	28	Super low	0.01210	18.183	0.1008	0.0079	4.6848

Table 2: Permeability grades of rocks.

Grades	1	2	3	4	5	6	7
Permeability	Super high	Very high	High	Medium	Low	Very low	Super low
Permeable area/10^{-3} μm^2	>1000	1000~500	500~100	100~50	50~10	10~1	<1

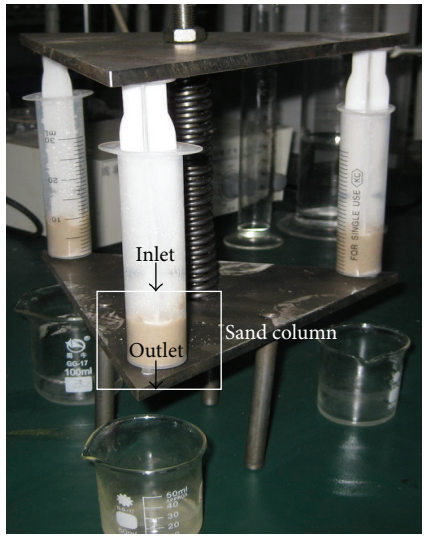

Figure 1: Photos of microbe-inspired $CaCO_3$ cementation.

vibrations into a plastic injection tube, 22 mm in diameter and 95 mm in length. Those tubes, filled with sand, were prepared for microbe-inspired $CaCO_3$ cementation [4]. This endeavor was a method of reaction fluid gravitational permease and external pressure [5]. It was to make the sand compact as much as possible under 0.1 MPa axial pressures during the whole cementation. An iron frame was designed to allow tubes to locate in it steadily and properly (Figure 1).

2.3. Mercury Intrusion Porosimetry Method. Porosimetry, such as pore diameter, total pore volume, superficial area, and pore throat ratio, was measured to demonstrate nano-$CaCO_3$-sand structure of samples taken as Figure 2 under PoreMaster-60 of Quantachrome, USA. The sizes and the sphere of distribution of pores and throats and their arrangement relating to each other were determined by mercury intrusion-extrusion capillary pressure curves. And the pore throat aspect ratio was that of pore radius to the relevant throat radius, which indicated their dimensional arrangement in material (Figure 3).

2.4. X-Ray Diffraction. Samples were taken from calcite precipitate in sand columns to make X-ray diffraction analysis. Grain size, phase retrieval, and lattice constant refinement were conducted on MDI JADE 5.

2.5. Transmission Electron Microscope. Calcite precipitate morphology was observed under Tecnai T20. The lattice diffraction pattern was taken to identify the phase of the precipitate with powder diffraction database of PCPDFWIN-2002.

2.6. Scanning Electron Microscope. SEM samples were taken from both ends and also from the middle part of the sand columns shown in Figure 5, to observe the amount and the location of the calcite precipitate under JSM-5900 of Siren, Japan.

3. Results and Discussion

The characterizations of the white precipitate in cementing the loose sand were discussed, focused on porosity and permeability, morphological observation phase identification, grain size calculation, and crystal type determination.

3.1. Porosity. As shown in Figure 2, from which MIP samples were taken, plenty of data were obtained from the porosity standard report of MIP, such as permeable area, total porosity volume, total porosity volume fraction, specific superficial area, and pore throat aspect ratio, all of which were listed in Table 1. Compared with the permeable area of grades in Table 2, permeability of all the sand columns fell into the super low grade.

The pore throat aspect ratio of sand columns at 672 hours sharply decreased to 0.49 from 3.83 at 120 hours (Figure 4). The pore throat aspect ratio indicated dimensional arrangement of pores and throats, and it explained the reduction of pore radius when more and more precipitation formed and filled in the pores with increasing cementation time.

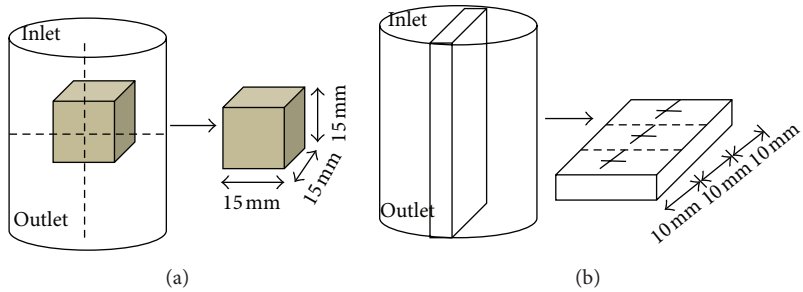

Figure 2: Sample taken places demonstration: (a) MIP samples, (b) SEM samples.

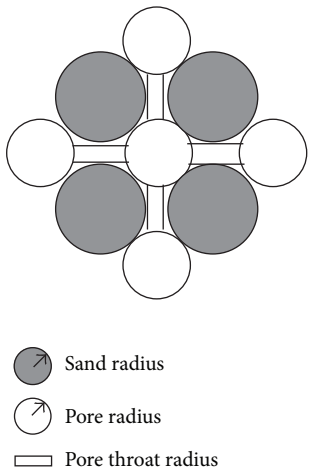

Figure 3: 2D sand, pore, and pore throat radius.

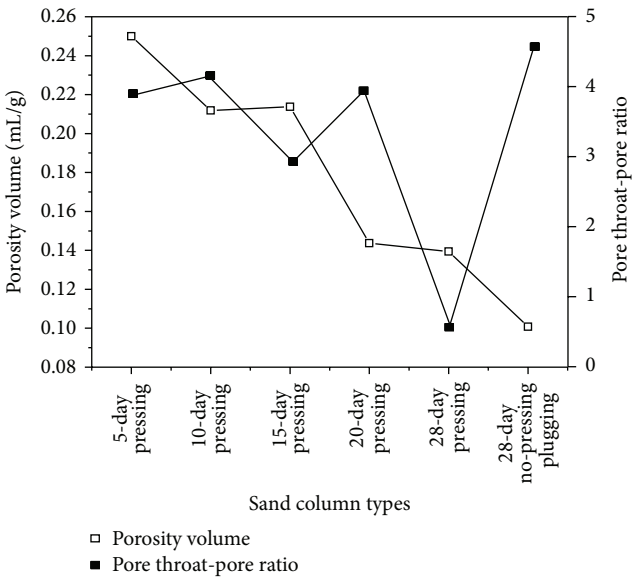

Figure 4: Porosity volume and pore throat aspect ratio of sand columns at different ages.

3.2. Morphological Observation

3.2.1. Precipitate Distribution. SEM samples were taken from the inlet, the middle, and the outlet part of white precipitate and sand, Figure 4. As shown in Figure 4, the amount of precipitate particles reduced constantly along the inlet, the middle, and the outlet, which explained why microbe-inspired precipitate reaction flew from the inlet to the outlet and quite amount of the calcite precipitate accumulated in the inlet area.

3.2.2. Particle Size. White precipitate particles exhibited a uniform distribution of about 15 μm size and of a hexahedral shape mostly in Figure 5. Since crystal growth is affected by various constraints, the irregular shape of the precipitate particles was due to the unequal compression in different parts of the sand column.

3.3. Phase Identification and Quantity Analysis

3.3.1. Phase Identification. X-ray diffraction pattern of the microbe-inspired precipitate was shown in Figure 5, indicating that the precipitate was calcium carbonate in calcite crystals.

3.3.2. Grain Size. Scherrer equation was introduced to calculate the average crystallite size of the calcite precipitate, as shown in

$$\beta = \frac{K\lambda}{L\cos\theta} + 4e\,\mathrm{tg}\,\theta \tag{5}$$

or

$$\frac{\beta\cos\theta}{\lambda} = \frac{K}{L} + \frac{4e\,\sin\theta}{\lambda} \tag{6}$$

wherein β, is the full width of the Bragg peak, as measured at half height, rad, θ, the Bragg peak angle, degree, λ, the wavelength of the radiation, Å, L, the average crystallite size, Å, e, the average crystallite size of distortion, Å, and K, a constant. The value depends on the method used and varies between 0.5 and 1 but is usually taken as around 0.9.

Calculation steps were as follows:

(a) determine λ as 1.5406 Å;

(b) set $Y = \beta\cos\theta/\lambda$, $X = \sin\theta/\lambda$, and the linear function was $Y = A + BX$, in which $A = K/L$ and $B = 4e$;

(c) while $K = 0.9$, $L = 18.5$ nm.

Calcium carbonate crystallite size based on the Scherrer equation was calculated for 18.5 nm.

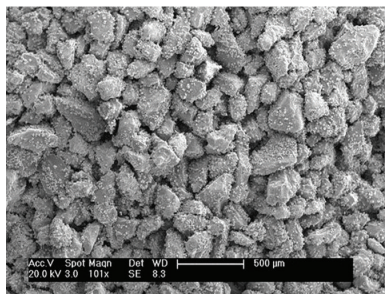

(a) The inlet

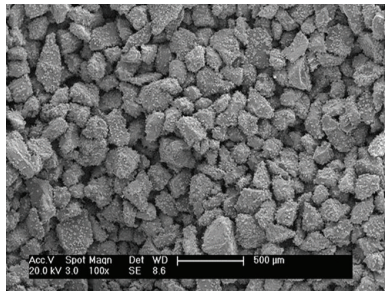

(b) The middle

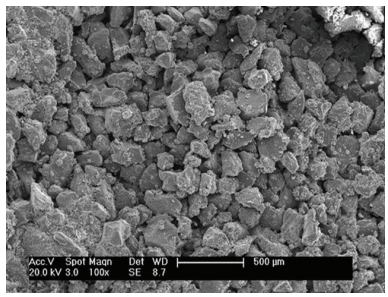

(c) The outlet

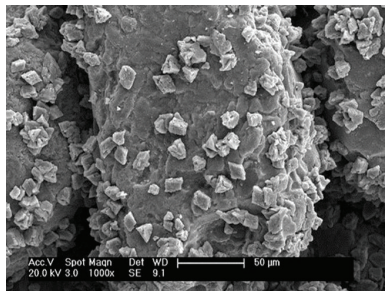

(d) White precipitate particles

FIGURE 5: SEM photos; white spots: calcite particles and grey irregular solids: sand particles.

3.4. Crystal Structure Analysis. TEM morphological photos were taken as shown in Figure 6 and the flaky outward growth of the nano-$CaCO_3$ was observed. The diffraction pattern of the nano-$CaCO_3$ was also taken to be analyzed as follows.

(a) Input the diffraction pattern into Photoshop CS5 and read data as follows: $x_1 = 516$ pixels, $y_1 = 1237$ pixels, $x_2 = 1968$ pixels, $y_2 = 915$ pixels, $n_1 = 7$, $x_3 = 725$ pixels, $y_3 = 380$ pixels, $x_4 = 1595$ pixels, $y_4 = 1802$ pixels, and $n_2 = 3$, as shown in Figure 7.

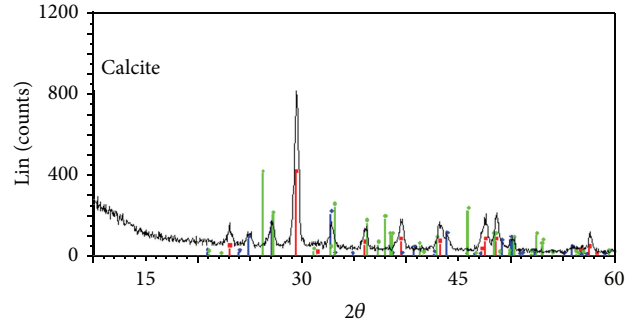

FIGURE 6: Microbe-inspired precipitate XRD.

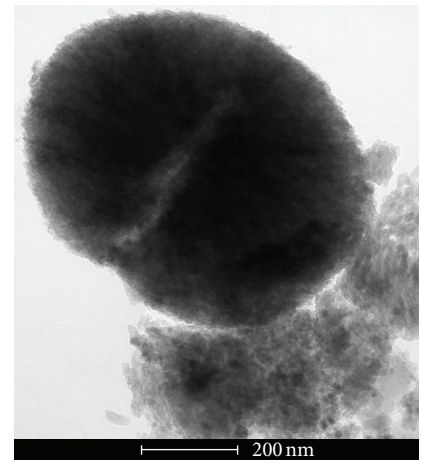

(a)

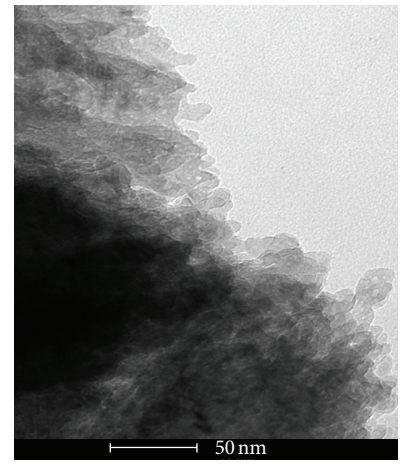

(b)

FIGURE 7: TEM morphological photos of white precipitate: (a) ×250, (b) ×1000.

(b) Input the above data into a self-edited calculation program in Matlab. The results were $d_1 = 3.0651$ Å, $d_2 = 3.0358$ Å, and $\theta = 74.5448^\circ$.

(c) Since $d_1/d_2 \approx 1$, $\theta = 74.5448^\circ$, $d_{1/a} = 0.9934$, and $a = 3.0450$ Å were deduced from the f_{cc} structure with the general error scope of 10% as a and 5% as θ.

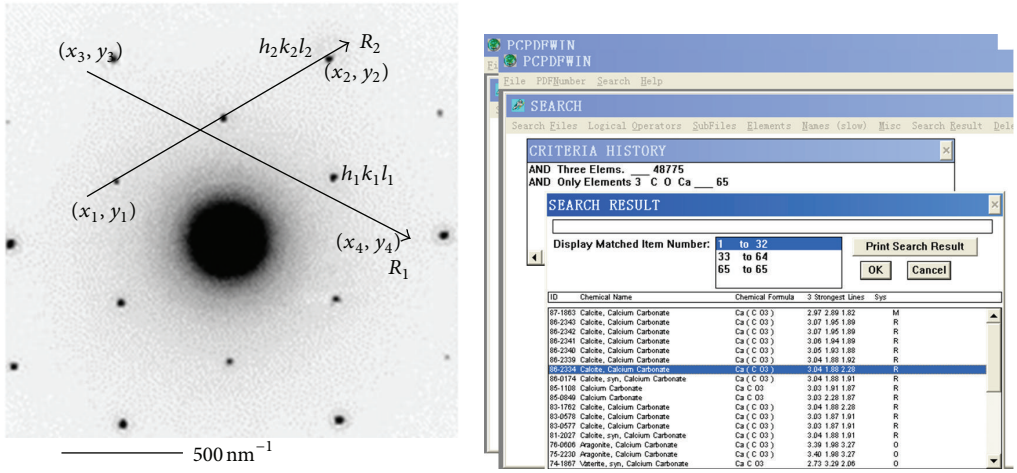

(a) (b)

FIGURE 8: (a) TEM diffraction pattern of $CaCO_3$ precipitate and (b) PCPDFWIN-2002 search result: ID 86-2334 calcite.

(d) In alignment with the 52 inorganic crystal composed of three elements of Ca, C, and O in PCPDFWIN-2002, the precipitate was identified as ID86-2334 calcite calcium carbonate, as shown in Figure 8.

4. Conclusion

This paper introduced an innovative bioengineering method of microbial carbonate precipitation in porous media [6]. The whole material preparation procedure incorporates the reaction fluid flow, solute transport, crystal growth, and deposition on sand grains. The final objective is an industry-scale application for geological material consolidation and strengthening, such as mineral plugging, immobilizing heavy metal ions in ground water, and strengthening of concrete or sand [7–11].

References

[1] P. Cacchio, C. Ercole, G. Cappuccio, and A. Lepidi, "Calcium carbonate precipitation by bacterial strains isolated from a limestone cave and from a loamy soil," *Geomicrobiology Journal*, vol. 20, no. 2, pp. 85–98, 2003.

[2] R. P. Reid, P. T. Visscher, A. W. Decho et al., "The role of microbes in accretion, lamination and early lithification of modern marine stromatolites," *Nature*, vol. 406, no. 6799, pp. 989–992, 2000.

[3] A. Sharma and A. Bhattacharya, "Enhanced biomimetic sequestration of CO_2 into $CaCO_3$ using purified carbonic anhydrase from indigenous bacterial strains," *Journal of Molecular Catalysis B*, vol. 67, no. 1-2, pp. 122–128, 2010.

[4] J. Geotech and E. Geoenvir, "Urease effects on urea hydrolysis," *Biological Considerations in Geotechnical Engineering*, vol. 131, no. 10, pp. 1222–1233, 2005.

[5] S. Stocks-Fischer, J. K. Galinat, and S. S. Bang, "Microbiological precipitation of $CaCO_3$," *Soil Biology and Biochemistry*, vol. 31, no. 11, pp. 1563–1571, 1999.

[6] H. Eccles, "Treatment of metal-contaminated wastes: why select a biological process?" *Trends in Biotechnology*, vol. 17, no. 12, pp. 462–465, 1999.

[7] S.-W. Lee, S.-B. Park, S.-K. Jeong, K.-S. Lim, S.-H. Lee, and M. C. Trachtenberg, "On carbon dioxide storage based on biomineralization strategies," *Micron*, vol. 41, no. 4, pp. 273–282, 2010.

[8] J. Dejong, "Microbially induced $CaCO_3$ cementation to improve soil behavior," *Sedimentary Geology*, vol. 2, pp. 769–773, 2007.

[9] V. S. Whiffin, M. P. Harkes, and L. A. van Paassen, "Microbial carbonate precipitation as a soil improvement technique," *Geomicrobiology Journal*, vol. 24, no. 5, pp. 417–423, 2007.

[10] L. Li, C. X. Qian, and R. X. Wang, "A lab investigation of MIP method used in Cd++ contaminated soil," *Journal of Soil and Sediments*, vol. 25, no. 2, pp. 331–335, 2010.

[11] J. K. Stolaroff, G. V. Lowry, and D. W. Keith, "Using CaO- and MgO-rich industrial waste streams for carbon sequestration," *Energy Conversion and Management*, vol. 46, no. 5, pp. 687–699, 2005.